Ocean Engineering 286 (2023) 115561

Contents lists available at ScienceDirect

Ocean Engineering

journal homepage: www.elsevier.com/locate/oceaneng

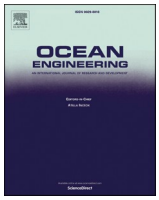

Powering performance prediction of a semi-displacement ship retrofitted with Hull Vane

Cihad Çelik [a,b,*], Devrim Bülent Danışman [b]

[a] Liverpool Logistics, Offshore and Marine (LOOM) Research Institute, Liverpool John Moores University, Liverpool, UK
[b] Istanbul Technical University, Faculty of Naval Architecture and Ocean Engineering, 34469, Istanbul, Turkey

A B S T R A C T

This study predicts the powering performance of a semi-displacement ship, both without and with a Hull Vane (HV). HV is an energy-saving appendage fixed at the transom bottom of the ship's hull. Although the HV is commercially known as a successful resistance-reducing device, there are no studies in the literature examining its effect on propulsion performance in detail. In this study, the effect of the HV on the propulsion performance is investigated and a practical method is proposed as an engineering application to reduce the computation time. Initially, the idealized disc model based on Blade Element Theory (BET) is preferred to create a thrust force instead of using an entire physical propeller. The dynamic motions of the ship are reflected in the computational analysis. Subsequently, the sliding mesh technique, which models the exact propeller geometry, is implemented to calculate the self-propulsion characteristics without and with HV. These computations are achieved by employing a two-phase flow solver available in OpenFOAM. This study provides a significant demonstration to clarify the effect of HV on powering performance. It not only decreases effective power by **11.41%** but also increases the propulsive efficiency by **2.1%**, which reduces the brake power by **14.61%** in total at service speed.

1. Introduction

The societal consciousness regarding the imperative to reduce carbon emissions is progressively escalating. The International Maritime Organization (IMO) is slated to implement new restrictive guidelines concerning carbon emissions in the forthcoming years. In the past decade, significant attention has been directed toward reducing ships' fuel consumption, which can be accomplished through various applications, including the utilization of energy-saving appendages and alternative energy sources. The utilization of appendages is a well-established practice to reduce a ship's resistance or increase its propulsive performance by directing the flow's streamlines and optimizing the pressure distribution on the ship's hull. Among these appendages is also the Hull Vane (HV), a transversely fixed hydrofoil wing at the bottom of a ship's transom. The working mechanism of the HV is founded on the concept that the low-pressure zone on the suction side of it absorbs the high-pressure zone located aft of the ship, thereby diminishing the hull resistance (Çelik et al., 2021). It is necessary to conduct an in-depth investigation into the impact of the HV not only on the ship resistance but also on the propulsive efficiency of the ship. Overall, the brake power prediction of the ship without and with HV indicates a satisfactory comparison. Predicting the ship's self-propulsion coefficients plays a critical role in calculating the brake power of its machinery. Two approaches commonly employed to predict these coefficients are self-propulsion experiments conducted in towing tanks and virtual towing tanks utilizing Computational Fluid Dynamics (CFD) simulations. The reliability of CFD studies on marine applications cannot be underestimated by considering advances in both commercial and open-source CFD packages.

Uithof et al. (2014) and Ferré et al. (2019) defined the advantages of the HV in terms of forward thrust, reduced wave-making, reduced running trim, and reduced motion in waves. The working principle of forward thrust by HV is based on the fact that when the horizontal component of the HV's lift force exceeds the horizontal component of the drag force, it produces an additional thrust force and modifies the vessel's trim through the vertical force. As a result, this yields a favorable impact on the overall resistance of the vessel. A series of numerical and experimental studies have been performed to investigate the HV impact regarding on ship resistance (Haywood and Ricks, 2021), seakeeping (Hou et al., 2020; Uithof et al., 2016), and fuel consumption (Bouckaert et al., 2016). As a result of the resistance simulations performed by Celik et al. (2020), the impact of the HV was predominantly noticed on the wave resistance in comparison to other resistance components, revealing a 31% decrease in contrast to the ship hull without HV on model scale. Hou et al. (2020) conducted an experimental investigation of the HV's impact on ship resistance. They proposed two

* Corresponding author. Liverpool Logistics, Offshore and Marine (LOOM) Research Institute, Liverpool John Moores University, Liverpool, UK.
E-mail addresses: C.Celik@2022.ljmu.ac.uk (C. Çelik), bulent.danisman@itu.edu.tr (D.B. Danışman).

https://doi.org/10.1016/j.oceaneng.2023.115561
Received 12 May 2023; Received in revised form 21 July 2023; Accepted 5 August 2023
Available online 11 August 2023

extrapolation methods from model scale to full-scale; the first one assumes the HV as a part of the ship hull and the other method considers the HV as an appendage. The total resistance was decreased by approximately 10% with the presence of the HV when both assumptions were implemented in calculations. Along with the resistance, the seakeeping performance of a ship is advantageously affected by the HV. The installation of the HV has been demonstrated to effectively mitigate the pitch and heave motion of ships, DTMB 5415 experimentally (Hou et al., 2020), and 108m Holland-Class OPVs numerically (Bouckaert et al., 2016), resulting in an enhanced level of comfort and operability. However, it is reported that the impact of the HV on the roll motion of the vessel is considered insignificant (Bouckaert et al., 2016). Recently, Hofman et al. (2022) aim to explore the feasibility of further reducing pitch and heave motions by enabling HV to rotate, thereby altering the lift of the HV. This innovative solution is known as Dynamic Hull Vane® (DHV), which has been developed by Hull Vane BV in collaboration with Naiad Dynamics US Inc, a supplier of ride control systems. The research employed CFD and strip theory computations and indicated the additional benefits of DHV. While the passive HV minimizes pitch motions by 5–20%, the DHV can reduce pitch motions by 30–50% in extreme situations. In addition to seakeeping performance, the annual fuel consumption is known to be reduced by the HV associated with the reduction in ship resistance. Bouckaert et al. (2015) illustrate that from the resistance point of view, the installation of a Hull Vane, along with a minor modification to the vessel's hull, can lead to a decrease in the overall fuel consumption by 12.5%. At the velocity which accounts for the majority of the yearly fuel consumption (17.5 knots). A systematic evaluation has been conducted by Uithof et al. (2017) to compare the impact of the HV with interceptors, trim wedges, and ballasting on the vessel's performance. The findings indicate that despite the discovery of decreased resistance for all the methods of trim correction, the HV accomplishes the greatest decrease in resistance for the majority of the velocity spectrum, with reductions in resistance reaching up to 32.4%. Çelik et al. (2021) presented a data-driven approach for optimizing the section shape of HV, which resulted in a 1.2% further reduction in total resistance when compared to the reference HV. In order to eliminate the time-consuming process of assessing the resistance of designs through a viscous flow solver, a Machine-Learning (ML) centered model has been created. This model is able to predict the total resistance of the hull when an HV is installed. When retrofitted to a vessel's transom, the HV typically increases the overall length of the vessel. Hagemeister et al. (2017) addressed whether comparable outcomes can be obtained with a new vessel by increasing its length by the same amount. The results indicated that the installation of an HV behind the transom is the most advantageous strategy in terms of reducing the fuel consumption of the vessel. Apart from the impact of HV on quantifiable contributions, Uithof et al. (2016) have figured out some of its unquantifiable impacts and advantages. These comprise a reduction in the engine room size, lower initial investment costs due to decreased engine power, diminution in the size and expenses of auxiliary machines, and tank volumes. These benefits have resulted in the creation of additional functional spaces.

In the preliminary design stage, experimental measurements can be complex and time-consuming. Consequently, CFD utilizing the Finite Volume Method (FVM) is increasingly being employed to examine the interaction between ships and propellers, as well as to derive the self-propulsion characteristics. There are different types of numerical representations for propellers. Generally, these representations are investigated in two groups: non-discretized propeller approaches and discretized propeller approaches. The former includes actuator disc models (Đurasević et al., 2022; Jasak et al., 2019; Villa et al., 2019) and body force models based on Blade Element Momentum Theory (BEMT) (Feng et al., 2020), while the latter covers Moving Reference Frame (MRF) (Sezen et al., 2021), sliding mesh (Kinaci et al., 2018; Sezen and Atlar, 2023; Wang et al., 2021), and overset mesh (Đurasević et al., 2022) techniques. For example, within the scope of non-discretized propeller approaches, Sezen et al. (2018) modeled the propeller as an actuator disc based on the body force method coupled with the experimental open water data. Bakica et al. (2019) represented using a pressure-jump actuator disk model that is designed to be idealized, enabling the use of a sizeable time step that is well-suited for naval hydrodynamics. This modeling approach preserves both accuracy and CPU time efficiency. Villa et al. (2019) introduced a novel approach to enrich the results obtained from a body force technique, with the objective of minimizing computational time without compromising any valuable findings. Feng et al. (2020) presented a novel approach utilizing a body force technique integrated with the blade element momentum theory (BEMT), taking into account the three-dimensional viscous effects in combination with the Reynolds-averaged Navier–-Stokes equations (RANS) solvers. To compute the thrust and torque distributions on the blade, the BEMT algorithm incorporates velocity correlations derived from CFD simulations at the virtual disk. The thrust and torque of the propulsion model were determined by integrating these distributions along the propeller's blade. Within the scope of discretized propeller approaches, Tacar et al. (2020) employed the MRF technique to acquire the open water data of a special propulsion system called the Gate Rudder System (GRS). Delen et al. (2021) utilized the sliding mesh technique to simulate the rotational motion of the propeller behind the hull at different geometrical scales. Đurasević et al. (2022) recently evaluated three numerical representations of propellers, namely a fully discretized propeller, along with two variations of actuator disc models. One variant of the actuator disc model solely captures the thrust effect on the fluid flow, whereas the other model incorporates both the thrust and torque effects. The use of an overset grid in fully discretizing a propeller model resulted in accurate predictions of local flow characteristics, as evidenced by a comparison of axial and in-plane velocity components behind the operating propeller. The self-propulsion simulations for a model-scale combatant ONR Tumblehome have been performed by two distinct propulsion models, the body force technique and the discretized propeller through sliding mesh technique, with a Froude number (Fr) of 0.20 (Zhang et al., 2021). According to the results, the accuracy of the discretized propeller model in predicting the propeller rate of revolution is higher than that of the body force model. Specifically, the difference in the propeller rotational speed between the CFD results obtained using the discretized propeller model and the experimental data is less than 2%. To enhance computational efficiency, some applications (Guo et al., 2018; Guo and Zou, 2021) incorporate a coupled version of MRF and sliding mesh techniques. This approach is particularly useful since the sliding mesh technique requires more computational time due to the complex interaction between the rotating and stationary regions. For instance, Guo and Zou (2021) studied a RANS-based investigation on the impact of the rudder on the propeller characteristics of a twin-screw ship when maneuvering. Two numerical schemes, MRF and sliding mesh, were employed to solve the flow field surrounding the rotating propeller. The MRF scheme was utilized to acquire an estimated initial flow field, while the SM scheme was employed for the succeeding unsteady simulation. Due to the higher applicability of CFD in comparison to experimental methods, scale effect studies (Can et al., 2020; Terziev et al., 2019, 2022) of marine vehicles have become increasingly widespread recently. Sezen et al. (2021) investigated the impact of the scale on the resistance and self-propulsion characteristics of the DARPA Suboff submarine hull form, with an additional objective of investigating the applicability of the 1978 ITTC performance prediction technique for predicting the power requirements of submarines. The propeller flow was represented by employing the discretized propeller geometry through the MRF approach. The findings suggest that the 1978 ITTC performance prediction method can be employed with a reasonable level of confidence to extrapolate the results from the model to full scale. Apart from the impact of the scale effect, CFD offers high resolution and accuracy in predicting the self-propulsion characteristics of ships that have unconventional propulsion systems. The installation of energy-saving devices

(ESD) results in a rise in the propulsive efficiency of vessels, leading to a reduction in fuel consumption. Özsayan et al. (2022) computationally explored different pre-swirl stator (PSS) and duct designs to evaluate their impact on the propulsive efficiency of a 7000DWT INSEAN Tanker on model scale. Wang et al. (2021) conducted a comparison of the propulsive efficiency of vessels utilizing single-screw propulsion and those employing hybrid contra-rotating podded propulsion. Simulations of propeller configurations have been performed by sliding mesh technique. According to the RANS-based numerical findings, the vessel utilizing hybrid CRP podded propulsion exhibited a significantly greater effective wake fraction, a considerably reduced thrust deduction fraction, a superior hull efficiency, and an overall propulsive efficiency that was 4.12% greater when compared with the single-screw vessel.

The inventors of HV have conducted various experimental and computational studies on resistance and seakeeping performance of it (Bouckaert et al., 2016; Haywood and Ricks, 2021), but not on propulsive performance. To the best of both authors' knowledge, there is no available study investigating the effect of HV on propulsive performance in literature. Here, we propose an approach to estimate the self-propulsion characteristics of a ship equipped with HV concerning the ship's dynamic motions in the open-source CFD code, OpenFOAM. Firstly, the trim and sinkage of the ship are determined at the self-propulsion load by the idealized disc approach. Then, the ship's position is updated in global coordinates. Finally, self-propulsion simulations with a fully discretized propeller through the sliding mesh technique are carried out to calculate the propulsion factors. This study also offers an approach for the extrapolation of the HV from model scale to full scale. Whether HV is an appendage or acts as a part of the ship hull in the extrapolation process is compared with the full-scale resistance simulations.

2. Numerical model and methodology

A twin-screwed semi-displacement ship is considered a reference test case for propulsive performance analysis. The waterline length (L_{WL}) and Froude number (Fr) at service speed are 3.5 m and 0.37. Table 1 shows the main dimensions of the ship and Fig. 1 depicts the ship's geometry equipped with shafts, brackets, struts, and HV. Shapewise, HV is a hydrofoil wing transversely fixed at the transom bottom of the hull. The optimized version of HV's cross-section geometry created by Çelik et al. (2021) is used in the study. The chord length of HV is 2.9% of the L_{WL} and the angle of attack is 0 *deg* with respect to the calm waterline. Moreover, HV's span length is taken equal to the model's breadth. The leading edge of HV is positioned from the transom corner at a horizontal/vertical distance equal to 2.29% and 1.66% of the L_{WL}, respectively.

2.1. Numerical model

The open-source software, OpenFOAM version 9, is utilized as a viscous flow solver. The flow around the ship is solved as three-dimensional and incompressible by implementing finite volume discretization. The velocity and pressure fields are obtained through the numerical solution of the RANS equations and the continuity equation.

Table 1
Main particulars of the ship.

Scale	λ	16.5	
Length on waterline	L_{WL} *(m)*	3.5	57.75
Breadth	B *(m)*	0.727	12.00
Draught (midship)	T *(m)*	0.212	3.50
Displacement volume	∇ *(m^3)*	0.268	1203.89
Displacement	Δ *(ton)*	0.268	1233.99
Wetted surface area	S *(m^2)*	2.769	753.86
Block coefficient	C_B	0.533	0.533
Longitudinal centre of buoyancy	L_{CB} *(m) (+ fwd)*	−0.160	−2.640
Longitudinal centre of floatation	L_{CF} *(m) (+ fwd)*	−0.348	−1.218
Service speed	V	2.15 m/s	17 kn
Froude number	Fr	0.37	0.37

Fig. 1. Hull geometry of the semi-displacement ship equipped with HV.

The Shear Stress Transport (SST) $k-\omega$ turbulence model is employed in order to solve the turbulence equations, where ω represents the specific dissipation rate. The Euler method corresponds to the transient first-order implicit scheme applied for the time derivative (Fan et al., 2021). Gauss linear scheme meaning central differencing is used for the gradient terms. The pressure-velocity coupling is solved by the PIMPLE algorithm. The heave and pitch motions are released both in calm-water and self-propulsion simulations in order to model the same situation as in towing tank experiments. The free surface is modeled by adopting the Volume of Fluid (VOF) technique. The "interFoam" solver is utilized to address the above-mentioned features for two incompressible isothermal immiscible fluids.

Half of the ship is discretized and solved for both calm-water and self-propulsion simulations in order to decrease the computational time. Inlet, outlet, bottom, top, and side boundaries are located at 3.6, 4.6, 2.9, 2.3, and 2.9 L_{WL} away from the ship model, which are suitable ranges according to the ITTC procedure and guidelines (ITTC, 2014) to avoid numerical reflection from the boundaries.

The sides and bottom boundaries of the computational domain are constrained with a symmetry condition. The fluxes and the normal components of all variables are set to zero at the symmetry plane. The Dirichlet and Neumann boundary conditions are represented by a fixed value and zero gradients. The outlet phase means velocity and pressure inlet-outlet velocity applies zero gradients for outflow. The fixed flux pressure sets the pressure gradient on the boundary by the velocity boundary condition. The total pressure is calculated by adding static pressure to dynamic pressure. The inlet-outlet condition provides a zero gradient outflow condition. The frequency, turbulence eddy viscosity, and turbulence kinetic energy wall functions are represented by omegaWallFunction, nutkWallFunction, and kqRWallFunction, respectively. Table 2 shows boundary conditions for different parts of the computational domain considering the turbulence characteristics and fluid properties. These include velocity (U), pressure (p_rgh), phase fraction (alpha.water), turbulent kinetic energy (k), wall function model (nut), and turbulence specific dissipation rate (omega). Various acronyms are used in the remaining columns of the table as follows: FV: Fixed Value, ZG: Zero Gradient, PIOV: Pressure Inlet Outlet Velocity, MWV: Moving Wall Velocity, FFP: Fixed Flux Pressure, TP: Total Pressure, and IO: Inlet-Outlet conditions, VHFR: Variable Height Flow Rate, PEP: p_rgh Entrainment Pressure, OPMV: Outlet Phase Mean Velocity (Çelik et al., 2021).

Mesh generation is executed by blockMesh, topoSet, and snappyHexMesh utilities in OpenFOAM. Firstly, the control volume boundaries are arranged in the blockMesh file. The mesh density around the ship hull is increased gradually with the help of nested topoSets. Surface

Table 2
Boundary conditions.

	Inlet	Outlet	Atmosphere	Hull
U	FV	OPMV	PIOV	MWV
p_rgh	FFP	ZG	PEP	FFP
αlpha.water	FV	VHFR	IO	ZG
k	FV	IO	IO	kqRWF
nut	FV	ZG	ZG	nutkRWF
omega	FV	IO	IO	omegaWF

refinements, box refinements, and prism layers are achieved by implementing the snappyHexMesh utility. The mesh structure around the free surface and appendages is depicted in Fig. 2. After conducting a self-propulsion simulation through the sliding mesh technique, the computed average wall y + distribution along the hull, appendages, and HV is approximately 27. On the propeller surface, the average distribution is 3, due to the specific treatment applied to capture the flow characteristics more efficiently.

2.1.1. rotorDisk approach

In this study, the rotorDisk model is utilized as an idealized disc approach. The model is based on the Blade Element Theory (BET) which considers the propeller's effect on the flow instead of using a physical propeller. This method inserts the forces and moments of the propeller's blades as source terms into the momentum equations. The rotating region is defined within the actual propeller region and its diameter corresponds to the diameter of the propeller. It provides a resulting propeller wake. This approach is cheaper than simulating a physical propeller in terms of computational time (Patrao, 2017).

The propeller blade can be divided into a series of two-dimensional sections. The blade sectional thrust (dT) and torque (dQ) are calculated with the local velocity (W), flow angle ($\varnothing$), section angle (β), chord length (c), lift (c_l) and drag (c_d) coefficients of section.

$$\alpha = \beta - \varnothing \tag{1}$$

The angle-of-attack (α) is a dependent variable for the lift and drag coefficients of a section profile. These coefficients are defined as a table in the numerical model.

$$c_l = f(\alpha) \tag{2}$$

$$c_d = f(\alpha) \tag{3}$$

The axial (f_z) and tangential (f_θ) forces of the blade section are calculated as;

$$f_z = \frac{1}{2}\rho W^2 c(c_l \cos\varnothing - c_d \sin\varnothing) \tag{4}$$

$$f_\theta = \frac{1}{2}\rho W^2 c(c_l \sin\varnothing + c_d \cos\varnothing) \tag{5}$$

Generated thrust (T) and torque (Q) are calculated by integrating **equations 4** and **5** from the propeller hub to the tip.

$$T = \int_{r=hub}^{r=tip} f_z dr \tag{6}$$

$$Q = \int_{r=hub}^{r=tip} f_\theta r dr \tag{7}$$

The rotorDisk model is implemented utilizing the *fvModels* library in numerical code. It is essential to incorporate the propeller's characteristics and its configuration into the *fvModels* file. This model inserts the forces and moments calculated based on the BET as source terms into the momentum equations. The propeller's main particulars serve as input in the *fvModels* file can be seen in Table 3. The angle (β) of the blade's sections is set to 30 *deg* at the propeller hub and the tip. The drag and lift coefficients of the hydrofoil used as a blade section are given in Appendix A (Table A1). Additionally, the inclination angle of the propeller shaft is 3 *deg* with respect to the baseline. Accordingly, the rotorDisk zone is defined considering the shaft angle and propeller diameter which can be seen in Fig. 3.

2.1.2. Sliding mesh approach

Computational solutions for complex rotational flow interaction problems typically employ the sliding mesh technique. Due to the complex interaction between the propeller, hull, and HV in this study, the sliding mesh technique is preferred to predict the self-propulsion characteristics. A cylindrical region is defined around the propeller called a rotor region that rotates in every time step around the specified origin point (Mehdipour, 2014). The propeller geometry is fully discretized in it. The remaining stationary domain outside the cylindrical region is known as the stator region, encompassing the discretized hull, appendages, and rudders. The information between the rotor and stator regions is transferred through Arbitrary Mesh Interface (AMI) in every time step (Wilhelm, 2015). Fig. 4 shows the fully discretized propeller, appendages, hull, and HV configuration.

Table 3
Main particulars of the stock propeller.

Diameter	D (m)	0.13
Pitch ratio	P/D	0.844
Number of blades	Z	3
Hub diameter	D_H (m)	0.02
Expanded area ratio	A_E/A_0	0.85

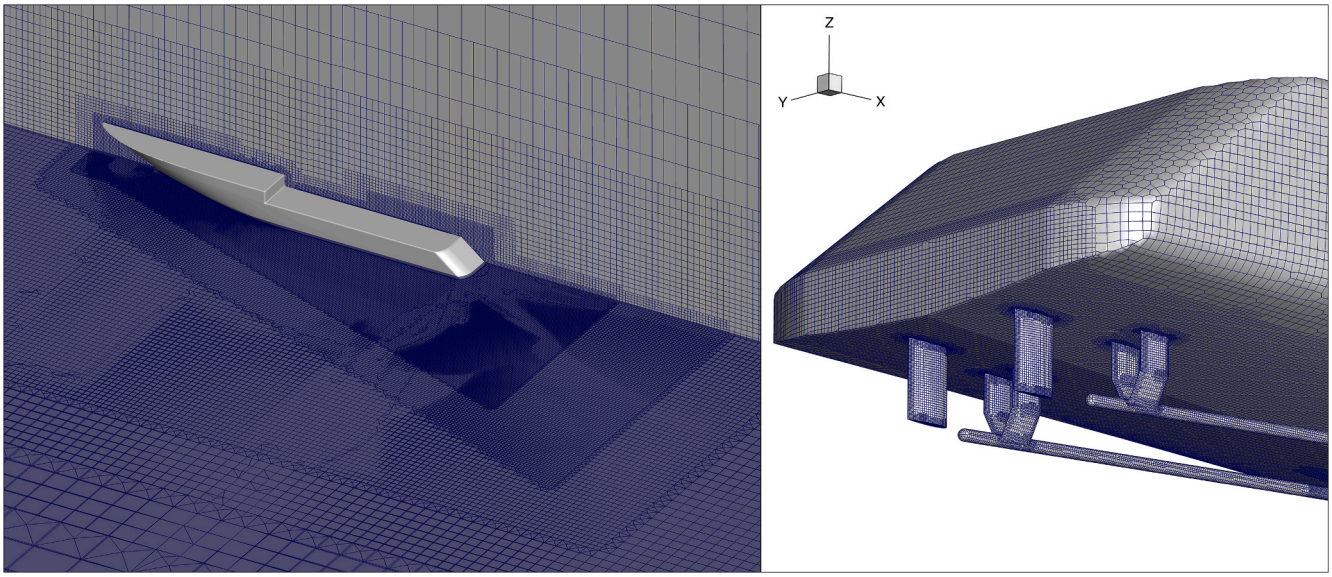

Fig. 2. Mesh layout around the free surface and appendages.

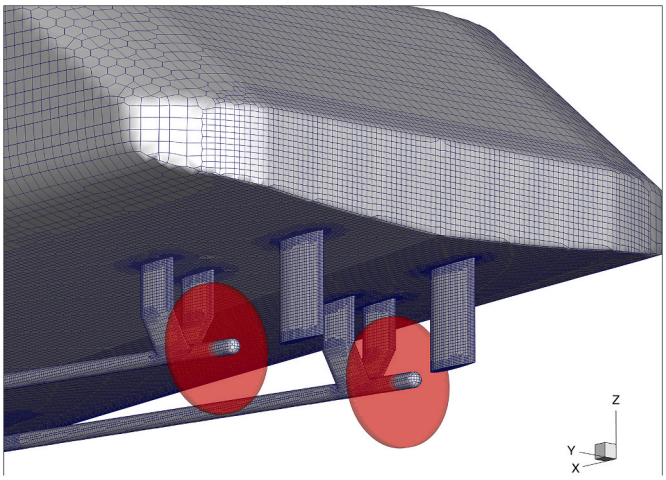

Fig. 3. RotorDisk configuration.

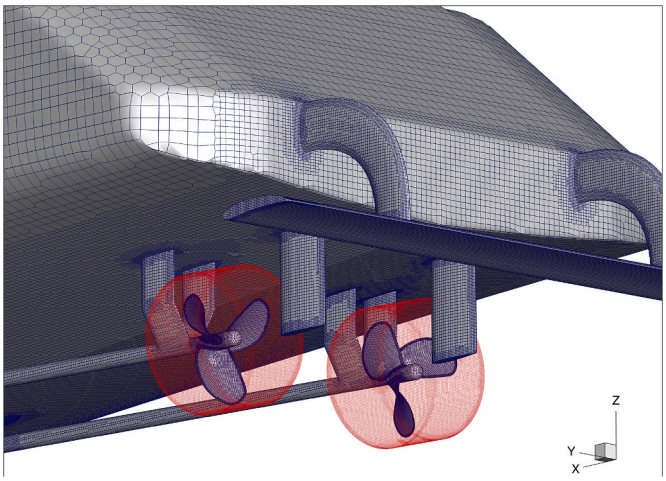

Fig. 4. Discretized propeller geometry in sliding mesh simulations.

2.2. Methodology

To predict the ship's performance without and with HV, resistance and self-propulsion simulations have been conducted separately, and then resistance results were evaluated in the ITTC 1978 prediction method.

Initially, resistance analyses of the hull without and with HV (Fig. 5 (a) and **(b)**) have been performed on model scale of 16.5. Moreover, full-scale analyses have been conducted at the service speed of 17 knots to determine the extrapolation process of the HV-installed ship. Then, model scale resistance analyses of the appended hull involving shafts and brackets without and with HV (Fig. 5 (c) and **(d)**) have been performed regarding the numerical procedure described in Section 2.1.

In self-propulsion simulations, the rotorDisk approach allowing the ship's dynamic motions was utilized instead of a fully discretized propeller. The appended ship model without and with HV has been simulated by rotorDisk at self-propulsion loadings to determine the dynamic trim and sinkage when the simulation converged. Subsequently, the dynamic motions of the ship model were updated and fixed in global coordinates. The propeller, appendages, and hull without and with HV were fully re-discretized in sliding mesh-based propulsion simulations. The thrust and torque values of the propeller were directly measured from the simulations which were used to derive the propulsion factors, t, w_t, and η_R. Open water data of the stock propeller was used in the prediction calculations. The flowchart of the detailed solution methodology is shown in Fig. 5. The subsections of Section 3 are encircled on the flowchart. Furthermore, the variations in geometrical configurations between the referred cases in the text are illustrated below the flowchart.

Computing resources used in this work were provided by the National Center for High Performance Computing of Turkey (UHeM). The technical specifications of the hardware server used for the code implementation and the materialization of the experiments scheduled in the context of the proposed approach are as follows; AMD EPYC™ 7742 type processor, 128 number of compute cores and Red Hat Enterprise Linux 8.5 operating system. The total computational time of a simulation by the rotorDisk approach and sliding mesh approach is approximately 210 and 190 min, respectively. The total computation time is around 400 min to measure the propeller thrust, torque values, and the forces on the ship hull, which are used to derive the propulsion factors.

3. Results and discussions

3.1. Model-scale resistance

Mesh generation steps, which were given in Section 2, were followed in pre-processing of resistance and self-propulsion simulations. Boundary conditions described in Table 2 were also maintained in all simulations. The uncertainty in spatial discretization was evaluated regarding the resistance results of the appended hull without HV. The steps of the uncertainty estimation procedure (Celik et al., 2008) are shown in Table 4. The fine grid convergence index was estimated as 1.5% with monotonic convergence performance. The index value is slightly higher than the index of spatial uncertainty estimation by Çelik et al. (2021) for the same reference ship, despite being generated a similar mesh structure for base size. This might be because the ship is equipped with appendages, which are the only difference in the current uncertainty estimation. The CFD simulations were performed with the mesh features used in the fine domain.

The resistance and self-propulsion experiments of the ship model without HV along with the nominal wake measurements have been conducted at Ata Nutku Ship Model Test Laboratory of Istanbul Technical University. Firstly, the resistance simulations of the ship model without HV have been performed and compared with the experimental results (see Fig. 8). CFD simulations show good agreement with the experiments, revealing a difference of **1.54%** in R_{TM} at service speed. Besides, a comparison of wave elevations can be seen in Fig. 6. The nominal wake distribution obtained from the CFD was validated with the experimental wake distribution, projecting similar patterns behind the brackets and shaft (see Fig. 7). Subsequently, the resistance simulations of the hull equipped with HV have been conducted to compare with the bare hull on model scale. The R_{TM} has been decreased by **11.20%** with the effect of HV at service speed. Specifically, a significant proportion of the reduction resulted from the wave resistance, which was also proved by Çelik et al. (2021). Fig. 8 shows the comparison of resistance curves for the ship without and with HV on model scale.

3.2. Full-scale extrapolation analysis of the HV

Full-scale extrapolation of the ship model with HV remains a topic requiring further investigation. Hou et al. (2020) proposed and compared two full-scale extrapolation methods, one considers the HV as a part of the ship hull (*Method I*), while the other is assuming HV as an appendage (*Method II*). It is still challenging to decide the best method due to the lack of full-scale measurements. In order to address this gap, we have carried out full-scale resistance simulations without and with HV at a service speed of 17 knots.

The resistance simulations of the hull without and with HV ((a) and (b) in Fig. 5) have been conducted without the shaft and brackets. Because the interaction between the appendages and the HV makes the interpretation of the HV impact on total resistance more challenging. To

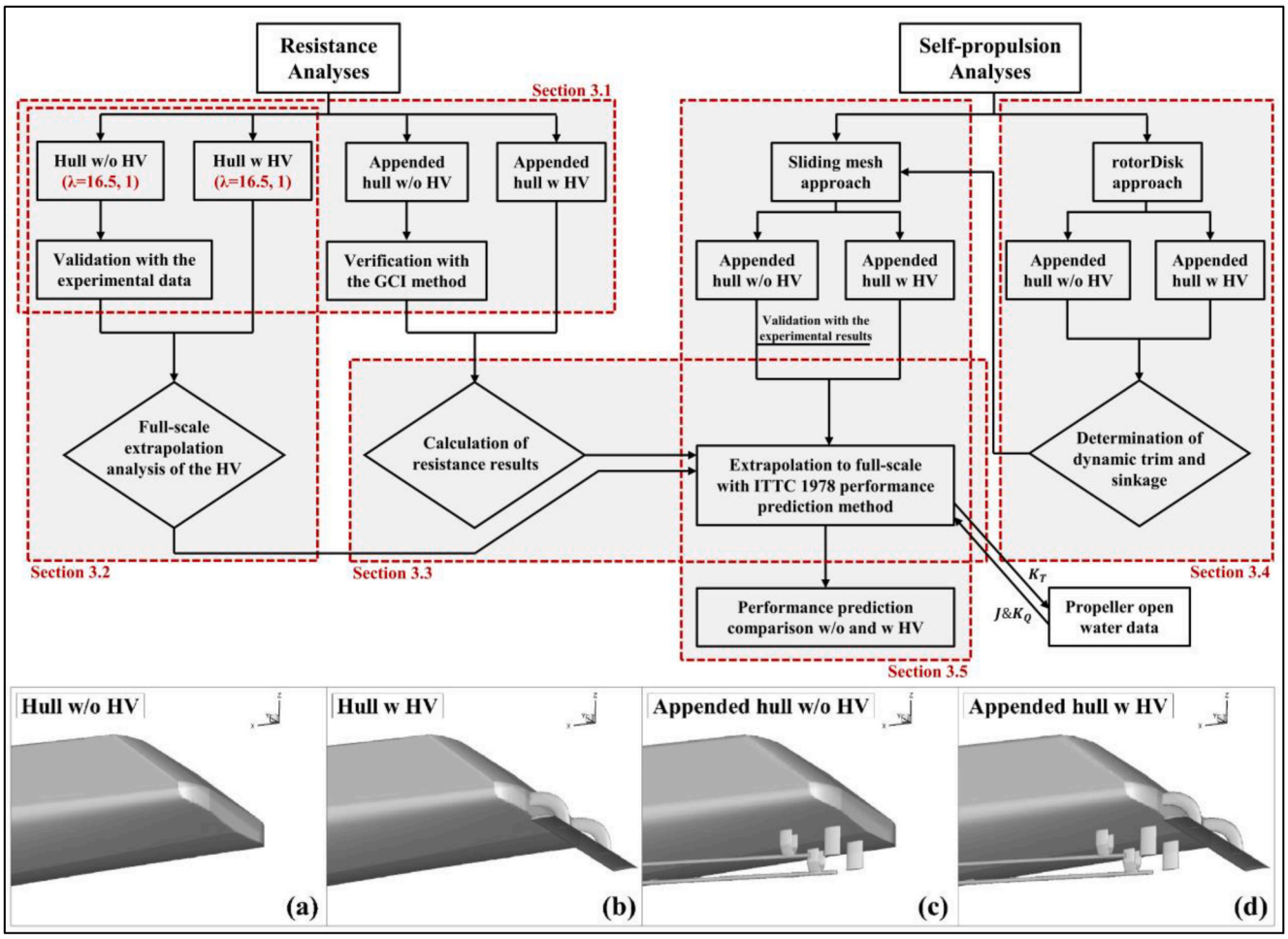

Fig. 5. The flowchart of the solution methodology.

Table 4
Uncertainty of spatial discretization.

Number of mesh	Fine	2795900
	Medium	1620155
	Coarse	938382
Refinement factor	r_{21}	1.20
	r_{32}	1.20
Total resistance	R_{TM1}	64.9168
	R_{TM2}	65.0151
	R_{TM3}	65.1263
Apparent order	p	0.673
Extrapolated value	$\varphi^{21}{}_{ext}$	64.1615
Approximate relative error	(%) e_a^{21}	0.15
Extrapolated relative error	(%) e_{ext}^{21}	1.18
Fine grid convergence index	(%) GCI_{fine}^{21}	1.5

predict the total resistance (R_{TS}), two proposed extrapolation methods have been implemented in the current study from model to full scale following the ITTC recommended procedure (ITTC, 2017b). It is a reminder that subscripts *M* and *S* refer to the model scale and full-scale ship in the rest of the paper.

$$R_{TS} = 0.5\rho_S S_S V_S^2 C_{TS} \tag{8}$$

Where, ρ_S, V_S, and S_S are the sea-water density at 15 °*C*, ship speed, and wetted surface area, respectively. C_{TS} is the total resistance coefficient without considering the roughness effect at this stage.

$$C_{TS} = (1+k)C_{FS} + C_W + C_{APPS} \tag{9}$$

$(1+k)$ is the form factor calculated in Çelik et al. (2021) for the same ship model. C_{FS} is the frictional resistance coefficient, C_W is the wave resistance coefficient, and C_{APPS} is the appendage resistance coefficient. C_{FS} is calculated according to ITTC 57 model-ship correlation line.

$$C_{FS} = \frac{0.075}{(log\ Re_S - 2)^2} \tag{10}$$

Re_S is the Reynolds number on full scale.

The C_W is calculated from model scale resistance simulations assuming the constant form factor.

$$C_W = C_{TM} - (1+k)C_{FM} - C_{APPM} \tag{11}$$

C_{FM} is calculated using equation (10) for the model scale. C_{TM} and C_{APPM} are calculated in equations (12) and (13).

$$C_{TM} = \frac{R_{TM}}{\frac{1}{2}\rho_M S_M V_M^2} \tag{12}$$

$$C_{APPM} = \frac{R_{TAPP}}{\frac{1}{2}\rho_M S_M V_M^2} \tag{13}$$

R_{TS} and R_{TAPP} are read off from the simulations. The scaling of appendage resistance is performed assuming a fixed fraction.

$$C_{AAPS} = (1-\beta)C_{APPM} \tag{14}$$

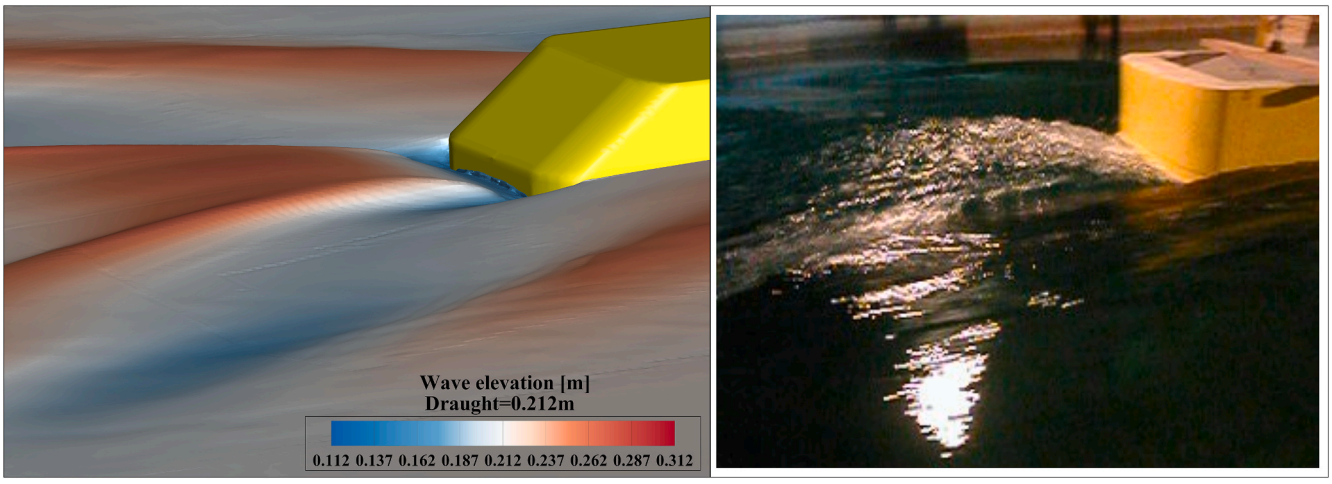

Fig. 6. Wave elevation of the ship model around the stern region.

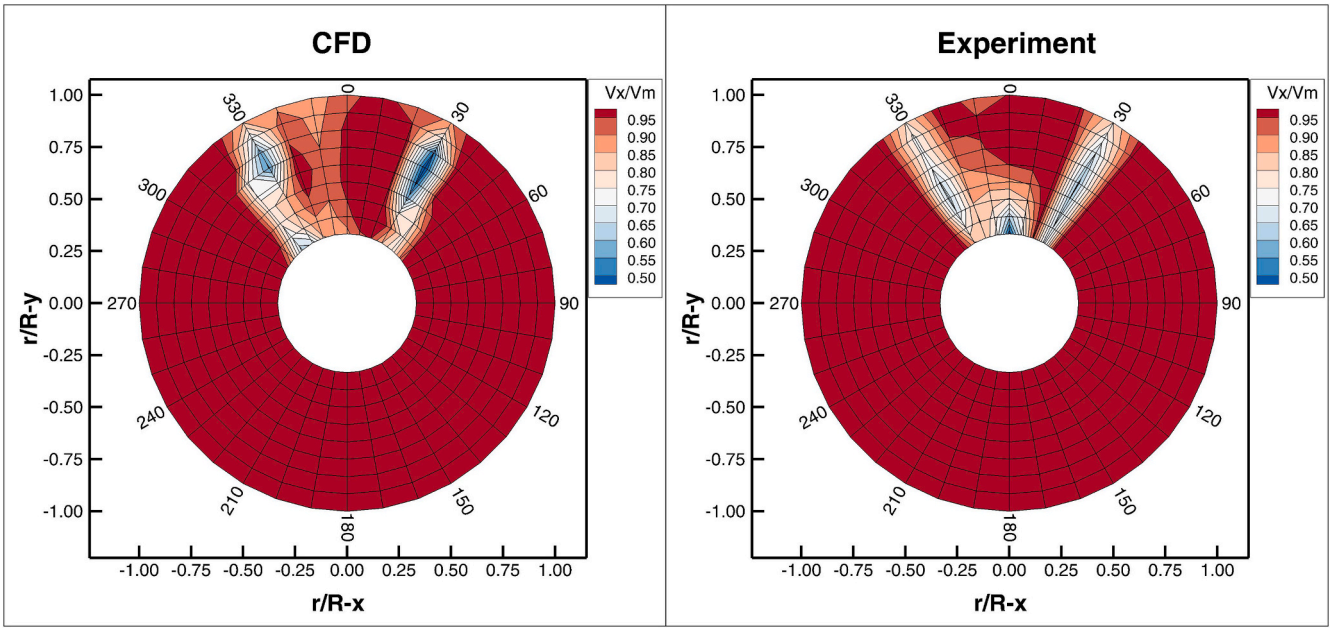

Fig. 7. Nominal wake distribution by CFD and experiment.

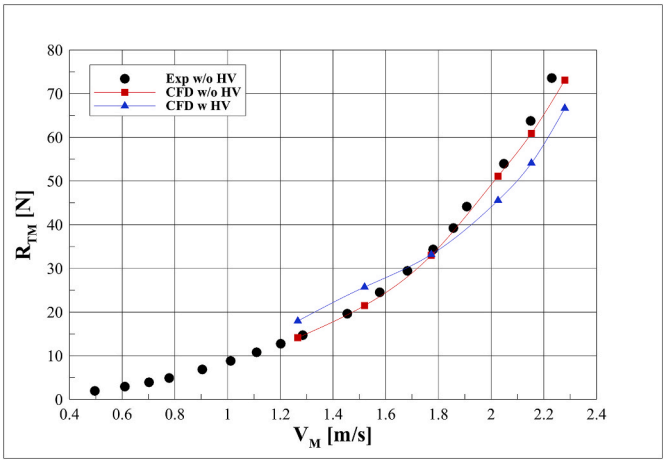

Fig. 8. Comparison of the resistance curves on model scale.

Here, $(1-\beta)$ is a constant value within the range between 0.6 and 1.0 defined by the procedure. Based on the experience in Ata Nutku Ship Model Test Laboratory, the $(1-\beta)$ is taken as 0.7 in calculations.

In *Method I*, the HV is considered a part of the hull, therefore, the C_{APPM} and its related terms are ignored in the afore-defined equations. The R_{TS} covers the hull and HV resistances together. In *Method II*, however, the HV is taken as an appendage in the extrapolation calculations. The resistance on the hull (R_{TS}) and HV (R_{TAPP}) is read from simulations separately.

A comparison between the extrapolated and full-scale CFD results is shown in Table 5. Here, both methods predict close results in full-scale resistance extrapolation, showing approximately 15% resistance reduction due to the presence of the HV. If the HV is considered as an appendage (*Method II*), the predicted results are more in line with the full-scale simulation result. Therefore, the HV in the extrapolation process was assumed as an appendage within the context of this study. Extrapolated R_{TS} results without and with HV are presented with full-scale measurements at service speed in Fig. 9. The impact of the HV on the wave elevation of the full-scale ship can be seen in Fig. 10. After

Table 5
Predicted and full-scale CFD results at service speed.

	Extrapolation							Full-scale CFD
	V_S[knot]	10^3C_{FM}	10^3C_W	10^3C_{FS}	10^3C_{AAPS}	10^3C_{TS}	R_{TS}[kN]	R_{TS}[kN]
Bare Hull	17.0	3.232	6.266	1.709	–	7.975	235.95	245.13
Method I	17.0	3.232	4.694	1.709	–	6.403	201.59	190.76
Method II	17.0	3.232	4.312	1.709	0.267	6.288	197.98	

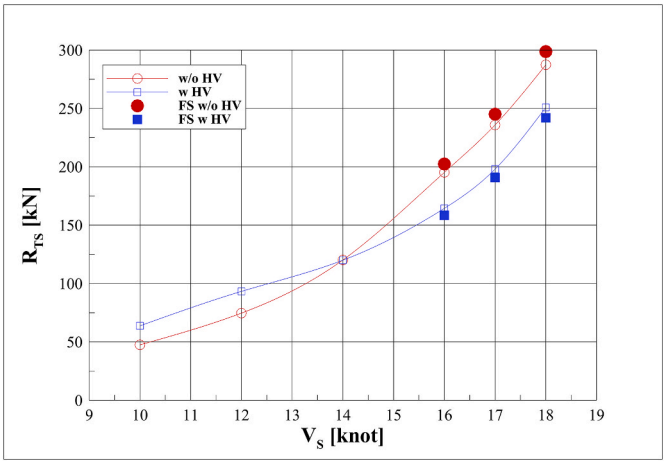

Fig. 9. Comparison of the extrapolated results by *Method II* and full-scale CFD results.

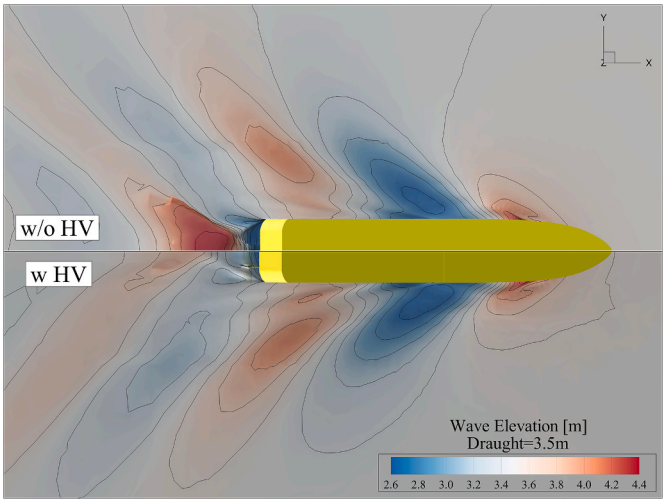

Fig. 10. Full-scale wave elevation without and with HV.

deciding on the suitable extrapolation method in this section, however, the extrapolation analysis is fully covered in **Section 3.3** including the resistance of the appendages and the roughness allowances.

3.3. Effective power predictions

Following the procedure (ITTC, 2017a), the C_{TS} is calculated including the C_{FS}, C_W, roughness allowance (ΔC_F), correlation allowance (C_A), and appendage resistance coefficient (C_{APPS}).

$$C_{TS} = (1+k)C_{FS} + C_W + \Delta C_F + C_A + C_{APPS} \tag{15}$$

The resistance of appendages (R_{TAPP}), including shaft, brackets, and HV if installed ((c) and (d) in Fig. 5), is measured from the simulation results. It is important to remind that S_M is updated according to the reference analysis. For instance, the wetted surface area of HV is included in the extrapolation process of the ship installed with HV.

$$\Delta C_F = 0.044\left[\left(\frac{k_S}{L_{WL}}\right)^{\frac{1}{3}} - 10Re^{-\frac{1}{3}}\right] + 0.000125 \tag{16}$$

The standard value of k_S is used as $150 \bullet 10^{-6}$.

$$C_A = (5.68 - 0.6logRe) \times 10^{-3} \tag{17}$$

Table 6 shows the comparison of the resistance coefficients and the predicted effective power (P_E) of the ship without and with HV. As a result, the P_E was decreased by **11.41%**.

3.4. Ship's dynamic motions

The ship's dynamic motions are affected by the presence of HV due to a negative pressure zone that appears on the top side of it (Çelik et al., 2021). Therefore, dynamic conditions have to be considered in propulsion analyses to properly calculate the ship's propulsion characteristics. The trim and sinkage of the ship model were calculated in resistance analyses. Here, the sinkage was decreased from 1.55 to 1.12 cm on model scale while the trim angle increased in the bow-down direction as a result of HV installation.

In this study, it is also taken the presence of the propeller into account, which has a direct impact on the ship's motions. As described in Section 2.1.2, instead of simulating the physical propeller with releasing dynamic ship motions which is extremely expensive in terms of computational time, the BET-based rotorDisk approach was implemented to model the propeller's impact on the flow around the stern region. The rotorDisk method allowing ship motions generates a favorable pressure distribution similar to that of the discretized propeller in both upstream and downstream directions. Additionally, it provides the necessary thrust force for self-propulsion operation. Compared to the resistance analyses, the sinkage of the ship model has slightly increased while the bow-down trim was decreased due to the effect of the propeller. A comparison of the ship's dynamic motions can be seen in Table 7. The sinkage and trim values of the ship model obtained with

Table 6
The effective power (P_E) predictions of the ship without and with HV.

	V_S[knot]	10^3C_{FM}	10^3C_W	10^3C_{FS}	$\Delta C_F + C_A$	10^3C_{AAPS}	10^3C_{TS}	P_E[kW]	Gain (%)
w/o HV	17.0	3.232	5.801	1.709	0.144	0.416	8.070	2195.39	
w HV	17.0	3.232	3.968	1.709	0.144	0.921	6.742	1944.98	11.41

Table 7
Dynamic trim angle and sinkage in resistance and rotorDisk propulsion simulations.

	Resistance		rotorDisk	
	Sinkage [cm]	Trim [deg]	Sinkage [cm]	Trim [deg]
w/o HV	1.55	−0.172	1.65	−0.073
w HV	1.12	−0.962	1.27	−0.818
				-: bow-down

rotorDisk simulations have been updated and fixed in global coordinates to perform further simulations by sliding mesh approach. Fig. 11 provides the axial velocity contours around the stern region by rotorDisk method at self-propulsion loadings.

3.5. Brake power predictions

Model test and sliding mesh-based CFD results were analyzed following the 1978 ITTC Performance Prediction Method (ITTC, 2017a). Thrust (T_M) and torque (Q_M) values were obtained at the self-propulsion point and expressed in the non-dimensional forms behind the hull conditions as K_{TM} and K_{QM}, respectively. Here, the **thrust identity** approach was used, in which J_{TM} and K_{QTM} corresponding to the K_{TM} are read off from the open water diagram of the stock propeller. J_{TM} and K_{QTM} are the propeller advance and torque coefficients in open water conditions. The wake fraction (w_{TM}) is calculated as;

$$w_{TM} = 1 - \frac{J_{TM} D_M n_M}{V_M} \tag{18}$$

Where, D_M, n_M, and V_M are the propeller diameter, propeller rate of revolution, and model speed. The relative rotative efficiency (η_R) is expressed as;

$$\eta_R = \frac{K_{QTM}}{K_{QM}} \tag{19}$$

The thrust deduction (t) is calculated as;

$$t = \frac{T_M + F_D - R_{TM}}{T_M} \tag{20}$$

R_{TM} is the total resistance that includes the resistance of appendages as well as the impact of HV on the total resistance if it is installed. F_D is the skin friction correction calculated as;

$$F_D = 1/2 \rho_M V_M^2 S_M [(1+k)(C_{FM} - C_{FS}) - \Delta C_F] \tag{21}$$

Due to the increased wetted surface area, S_M was updated for the HV-installed ship.

The ship has an open stern geometry and twin-screw propeller configuration. According to the procedure, the wake scale effect is usually small in this type of ship and w_{TS} can be assumed as;

$$w_{TS} = w_{TM} \tag{22}$$

The hull efficiency (η_H) is;

$$\eta_H = \frac{1-t}{1-w_{TS}} \tag{23}$$

The propulsive efficiency (η_D) defined by Birk (2019) can be calculated as;

$$\eta_D = \eta_H \eta_O \eta_R \tag{24}$$

η_O is the open water efficiency of the propeller.

Self-propulsion tests of the ship model without HV have been conducted both experimentally and numerically in order to validate the configuration of the numerical approach in terms of the numerical schemes and boundary conditions applied. The external tow force is also known as F_D was included in the calculation of the thrust deduction factor. In this study, the **load variation method** was applied which includes three different propeller rates of revolution keeping the model speed constant. The experimental and numerical results of the propulsion factors and efficiencies are shown in Table 8. The difference in η_D between the experiment and CFD is related to the η_H, since the wake fraction of the ship model without HV was overestimated by CFD. However, looking at the entire table, the prediction of self-propulsion characteristics by CFD is in line with the prediction by experiment under a certain level of difference for the ship model without HV. Then, the same numerical configuration was applied for the prediction of the self-propulsion characteristics of the ship model installed with the HV. In the calculation of the thrust deduction factor, the total resistance of the ship and the required thrust by the propeller decreased due to the

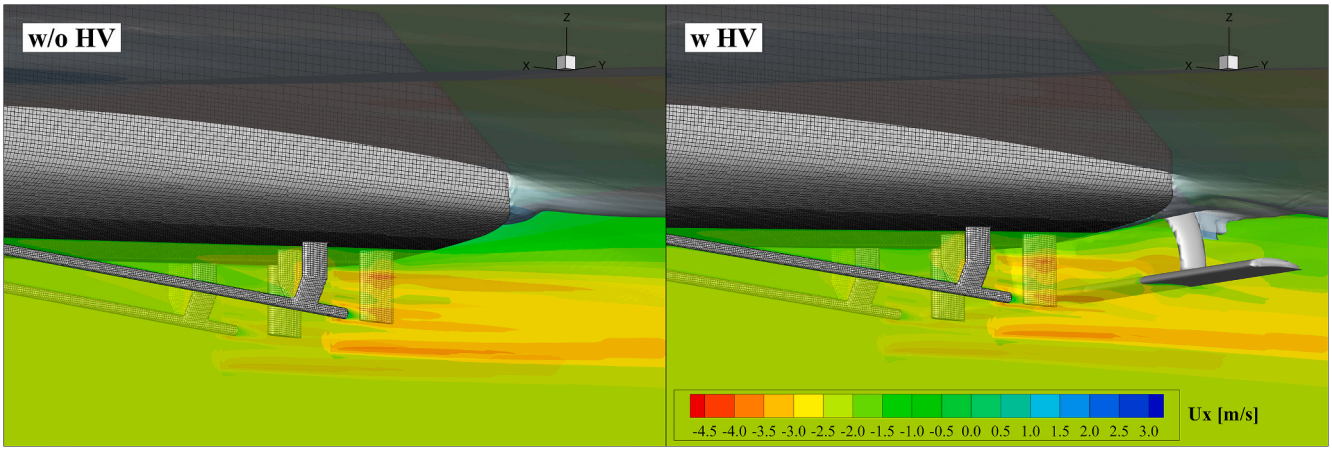

Fig. 11. Axial velocity contours by rotorDisk at self-propulsion loadings.

Table 8
Self-propulsion characteristics of the ship without and with HV at service speed of 17 knots.

	n(rps)	K_{TM}	$10K_{QM}$	J_M	t	w_{TS}	η_H	η_0	η_R	η_D
w/o HV (Exp.)	26.560	0.156	0.261	0.596	0.096	0.034	0.936	0.599	0.955	0.535
w/o HV (CFD)	26.428	0.157	0.260	0.574	0.088	0.052	0.962	0.605	0.941	0.547
w HV (CFD)	25.602	0.152	0.254	0.607	0.074	0.061	0.986	0.613	0.939	0.568

Table 9
The brake power predictions of the ship without and with HV.

	V_S[knot]	P_E[kW]	η_D	η_S	P_B[kW]	Gain (%)
w/o HV	17.0	2195.39	0.547	0.980	4092.33	
w HV	17.0	1944.98	0.568	0.980	3494.45	14.61

presence of the HV. F_D slightly increased for the HV-installed model because of the increased wetted surface area. Using **equation (20)**, t is calculated as 0.074. It is clear that the HV decreases the t, while increasing the w_{TS}, which improves the η_H. In this study, HV has been considered as a retrofit design means that the HV is installed on the existing ship in operation, therefore, the same stock propeller was used in the self-propulsion simulations. As a result, the K_{TM} has slightly decreased, which shifted the propeller advance coefficient towards the peak of the open water efficiency at service speed compared to the ship without HV. In total, the HV increased the propulsive efficiency by **2.1%** at service speed.

Finally, the brake power of the ship without and with HV was calculated with η_D and the shaft efficiency (η_S) using **equation (25)**. η_S was assumed as 0.98. Table 9 shows the comparison of the predicted results. As a result of the performance prediction analysis, there is a **14.61%** reduction in P_B when the ship is equipped with the HV as a retrofit energy-saving appendage at service speed.

$$P_B = \frac{P_E}{\eta_D \eta_S} \tag{25}$$

One further comparison was performed by calculating the vortex structures in the propeller slipstream direction at self-propulsion loadings. $Q = 3000\ 1/s^2$ was applied as a threshold value to visualize the vortex distribution. The flow velocity magnitudes were projected on the vortex pattern (see Fig. 12). It can be concluded that the HV also reduces the velocity magnitudes on the rudders, which may reduce the flow-induced vibration. However, detailed investigations are required to further interpret the HV's impact on hydroacoustics performance.

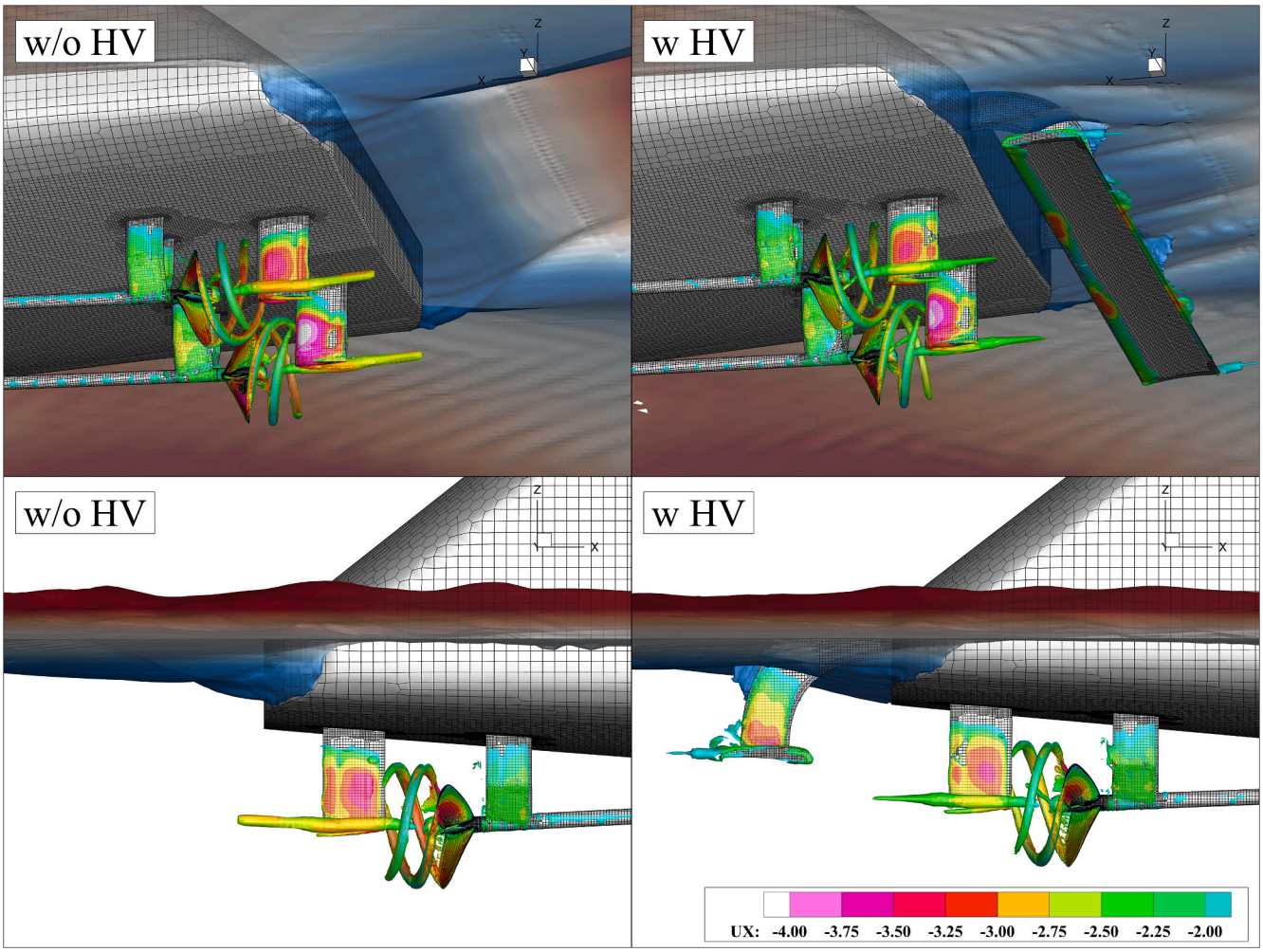

Fig. 12. The vortex structures in the propeller slipstream direction for the ship model without and with HV at self-propulsion points. ($Q = 3000\ 1/s^2$).

4. Conclusions

A great deal of emphasis is placed on the reduction of ships' fuel consumption, which can be achieved by employing energy-saving appendages. The present paper proposes an efficient methodology to predict the brake power of the ship equipped with an energy-saving appendage known as HV concerning the ship's dynamic motions. The methodology covers the determination of the ship's trim and sinkage at self-propulsion loadings by the BET-based rotorDisk approach. Subsequently, self-propulsion simulations are conducted with a fully discretized propeller in order to predict the propulsion factors of the ship with updated dynamic motions in global coordinates.

The extrapolation process of the ships installed with energy-saving appendages is generally questionable due to the lack of full-scale measurements. This study also offers a comprehensive extrapolation analysis of the ship retrofitted with HV from model to full scale. Two methods, the first one considers the HV to be a part of the ship hull, and the second assumes the HV is an appendage, are compared with the full-scale CFD resistance simulations. The results of the latter method are more in line with the full-scale total resistance measurements. As a result of the full-scale prediction, the effective power of the ship with HV is decreased by **11.41%** at a service speed of 17 knots.

The ship's dynamic motions are directly affected by the presence of HV and propeller. It is demonstrated that the corresponding trim and sinkage obtained from the rotorDisk simulations can be used as an input for the simulations with the sliding mesh approach to predict the propulsion factors accurately.

In propulsion analyses, it is evident that the HV causes a reduction in t, while leading to an increase in w_{TS}, thereby improving the η_H. In total, the HV increases the η_D by **2.1%** at service speed. Evaluating the effective power together with the η_D, the brake power of the ship with HV at the same reference speed is decreased by **14.61%**, which reduces the fuel consumption of the ship accordingly. A reduction of the velocity magnitudes is observed in the vortex structures around the propeller slipstream direction and rudders, which may help to reduce the flow-induced vibration around the stern part of the ship. However, further investigations with detailed computations are needed to confirm these findings.

CRediT authorship contribution statement

Cihad Çelik: Conceptualization, Methodology, Software, Formal analysis, Writing – original draft, Visualization. **Devrim Bülent Danışman:** Conceptualization, Methodology, Supervision, Writing – review & editing.

Declaration of competing interest

The authors declare that they have no known competing financial interests or personal relationships that could have appeared to influence the work reported in this paper.

Data availability

Data will be made available on request.

Acknowledgments

Computing resources used in this work were provided by the National Center for High Performance Computing of Turkey (UHeM) under grant number 4011962022.

Appendix A

Table A.1
Drag and lift coefficient of the blade section profile.

Angle of attack (α)	*Drag coefficient* (c_D)	*Lift coefficient* (c_L)
−90	0.210	1.45
−18	0.210	1.45
−16	0.165	1.30
−14	0.125	1.10
−12	0.092	0.95
−10	0.070	0.80
−8	0.050	0.64
−6	0.040	0.50
−4	0.028	0.32
−2	0.022	0.18
0	0.020	0.00
2	0.022	0.18
4	0.028	0.32
6	0.040	0.50
8	0.050	0.64
10	0.070	0.80
12	0.092	0.95
14	0.125	1.10
16	0.165	1.30
18	0.210	1.45
90	0.210	1.45

References

Bakica, A., Gatin, I., Vukčević, V., Jasak, H., Vladimir, N., 2019. Accurate assessment of ship-propulsion characteristics using CFD. Ocean Eng. 175, 149–162.

Birk, L., 2019. Fundamentals of Ship Hydrodynamics: Fluid Mechanics, Ship Resistance and Propulsion. John Wiley & Sons.

Bouckaert, B., Uithof, K., Moerke, N., Van Oossanen, P.G., 2016. Hull vane ® on 108m holland-class OPVs : effects on fuel consumption and seakeeping. In: Proceeding of MAST Conference 2016.

Bouckaert, B., Uithof, K., van Oossanen, P., Moerke, N., Nienhuis, B., van Bergen, J., 2015. A life-cycle cost analysis of the application of a Hull Vane® to an offshore patrol vessel. In: SNAME 13th International Conference on Fast Sea Transportation. FAST 2015. https://doi.org/10.5957/FAST-2015-028.

Can, U., Delen, C., Bal, S., 2020. Effective wake estimation of KCS hull at full-scale by GEOSIM method based on CFD. Ocean Eng. 218, 108052.
Celik, C., Danisman, D.B., Kaklis, P., Khan, S., 2020. An investigation into the effect of the hull vane on the ship resistance in openfoam. Sustainable Development and Innovations in Marine Technologies. In: Proceedings of the 18th International Congress of the International Maritime Association of the Mediterranean. IMAM 2019. https://doi.org/10.1201/9780367810085-17.
Çelik, C., Danışman, D.B., Khan, S., Kaklis, P., 2021. A reduced order data-driven method for resistance prediction and shape optimization of hull vane. Ocean Eng. 235 https://doi.org/10.1016/j.oceaneng.2021.109406.
Celik, I.B., Ghia, U., Roache, P.J., Freitas, C.J., Coleman, H., Raad, P.E., 2008. Procedure for estimation and reporting of uncertainty due to discretization in CFD applications. J.Fluid Eng. Transact. ASME 130 (7). https://doi.org/10.1115/1.2960953.
Delen, C., Can, U., Bal, S., 2021. Prediction of resistance and self-propulsion characteristics of a full-scale naval ship by CFD-based GEOSIM method. J. Ship Res. 65 (4), 346–361.
Đurasević, S., Gatin, I., Uroić, T., Jasak, H., 2022. Numerical analysis of self-propulsion flow characteristics in model scale. Ocean Eng. 259, 111885.
Fan, Y., Kunpeng, C., Weimin, C., Guoxiang, D., 2021. The effect of time discretization on the propeller hydrodynamic performance simulation in self-propulsion and open water conditions. J. Phys. Conf. 1834 (1), 012008.
Feng, D., Yu, J., He, R., Zhang, Z., Wang, X., 2020. Improved body force propulsion model for ship propeller simulation. Appl. Ocean Res. 104, 102328.
Ferré, H., Goubault, P., Yvin, C., Bouckaert, B., 2019. Improving the nautical performance of a surface ship with the Hull Vane ® appendage. ATMA 2738 (1).
Guo, H.-P., Zou, Z.-J., 2021. A RANS-based study of the impact of rudder on the propeller characteristics for a twin-screw ship during maneuvers. Ocean Eng. 239, 109848.
Guo, H., Zou, Z., Liu, Y., Wang, F., 2018. Investigation on hull-propeller-rudder interaction by RANS simulation of captive model tests for a twin-screw ship. Ocean Eng. 162, 259–273.
Hagemeister, N., Uithof, K., Bouckaert, B., Mikelic, A., 2017. Hull Vane® versus Lengthening: A Comparison between Four Alternatives for a 61m OPV.
Haywood, A., Ricks, A., 2021. Dynamic hull vane - a solution for active pitch motion reduction and resistance reduction of ships. In: SNAME International Conference on Fast Sea Transportation 2021. FAST 2021. https://doi.org/10.5957/FAST-2021-002.
Hofman, J., Haywood, A., Ricks, A., Bouckaert, B., 2022. Enhanced Dampening of the Pitch Motions with an Actively Controlled Hull Vane.
Hou, H., Krajewski, M., Ilter, Y.K., Day, S., Atlar, M., Shi, W., 2020. An experimental investigation of the impact of retrofitting an underwater stern foil on the resistance and motion. Ocean Eng. 205 https://doi.org/10.1016/j.oceaneng.2020.107290.
ITTC, 2014. ITTC-recommended procedures and guidelines practical guidelines for ship CFD applications. https://www.ittc.info/media/8165/75-03-02-03.pdf.
ITTC, 2017a. ITTC-recommended Procedures and Guidelines 1978 ITTC Performance Prediction Method.
ITTC, 2017b. ITTC-recommended procedures and guidelines resistance test. https://www.ittc.info/media/8001/75-02-02-01.pdf.
Jasak, H., Vukčević, V., Gatin, I., Lalović, I., 2019. CFD validation and grid sensitivity studies of full scale ship self propulsion. Int. J. Nav. Archit. Ocean Eng. 11 (1), 33–43.
Kinaci, O.K., Gokce, M.K., Alkan, A.D., Kukner, A., 2018. On self-propulsion assessment of marine vehicles. Brodogradnja: Teorija i Praksa Brodogradnje i Pomorske Tehnike 69 (4), 29–51.
Mehdipour, R., 2014. Simulating Propeller and Propeller-Hull Interaction in openFOAM.
Özsayan, S., Aydın, Ç., Köksal, Ç.S., Korkut, E., 2022. A systematic optimisation on the energy saving devices for ship. In: Particular, Combination of Pre-swirl Stator (PSS) and Duct.
Patrao, A.C., 2017. Description and validation of the rotorDiskSource class for propeller performance estimation. Proceed.CFD Open Source Softw.
Sezen, S., Atlar, M., 2023. Marine propeller underwater radiated noise prediction with the FWH acoustic analogy Part 1: assessment of model scale propeller hydroacoustic performance under uniform and inclined flow conditions. Ocean Eng. 279, 114552.
Sezen, S., Delen, C., Dogrul, A., Atlar, M., 2021. An investigation of scale effects on the self-propulsion characteristics of a submarine. Appl. Ocean Res. 113, 102728.
Sezen, S., Dogrul, A., Delen, C., Bal, S., 2018. Investigation of self-propulsion of DARPA Suboff by RANS method. Ocean Eng. 150, 258–271.
Tacar, Z., Sasaki, N., Atlar, M., Korkut, E., 2020. An investigation into effects of Gate Rudder® system on ship performance as a novel energy-saving and manoeuvring device. Ocean Eng. 218, 108250.
Terziev, M., Tezdogan, T., Incecik, A., 2019. A geosim analysis of ship resistance decomposition and scale effects with the aid of CFD. Appl. Ocean Res. 92, 101930.
Terziev, M., Tezdogan, T., Incecik, A., 2022. Scale effects and full-scale ship hydrodynamics: a review. Ocean Eng. 245, 110496.
Uithof, K., Bouckaert, B., Van Oossanen, P.G., Moerke, N., 2016a. A Cost-Benefit Analysis of Hull Vane Application on Motor Yachts.
Uithof, K., Bouckaert, B., Van Oossanen, P.G., Moerke, N., Hull Vane, B.V., 2016b. The Effects of the Hull Vane on Ship Motions of Ferries and Ropax Vessels. RINA, Royal Institution of Naval Architects - Design and Operation of Ferries and Ro-Pax Vessels, p. 2016.
Uithof, K., Hagemeister, N., Bouckaert, B., Van Oossanen, P.G., Moerke, N., 2017. A systematic comparison of the influence of the hull Vane®, inter-ceptors, trim wedges, and ballasting on the performance of the 50M amecrc series #13 patrol vessel. In: International Naval Engineering Conference. INEC@IMDEX Asia 2017, Singapore, pp. 17–18. May 2017.
Uithof, K., Van Oossanen, P., Moerke, N., Van Oossanen, P.G., Zaaijer, K.S., 2014. An update on the development of the Hull Vane®. In: 9 Th Int. Conf. On High-Performance Marine Vehicles (HIPER).
Villa, D., Gaggero, S., Gaggero, T., Tani, G., Vernengo, G., Viviani, M., 2019. An efficient and robust approach to predict ship self-propulsion coefficients. Appl. Ocean Res. 92, 101862.
Wang, Z., Min, S., Peng, F., Shen, X., 2021. Comparison of self-propulsion performance between vessels with single-screw propulsion and hybrid contra-rotating podded propulsion. Ocean Eng. 232, 109095.
Wilhelm, D., 2015. Rotating flow simulations with OpenFOAM. Int. J. Aeronaut. Sci. Aero. Res. 1, 001.
Zhang, Z., Liu, L., Yu, J., Yang, W., Zhang, Z., Jiang, K., 2021. Numerical simulation of ONR Tumblehome self-propulsion using discretized propeller and body-force models. In: The 31st International Ocean and Polar Engineering Conference.